Microrheology of isotropic and liquid-crystalline phases of hard rods by dynamic Monte Carlo simulations

Fabián A. García Daza[a,*], Antonio M. Puertas[b], Alejandro Cuetos[c] and Alessandro Patti[a,d,*]

[a]Department of Chemical Engineering, The University of Manchester, Manchester, M13 9PL, UK
[b]Department of Chemistry and Physics, University of Almería, 04120, Almería, Spain
[c]Department of Physical, Chemical and Natural Systems, Pablo de Olavide University, 41013, Sevilla, Spain
[d]Department of Applied Physics, University of Granada, Fuente Nueva s/n, 18071 Granada, Spain

ARTICLE INFO

Keywords:
Colloids
Liquid Crystals
Microrheology
Dynamic Monte Carlo simulations
Brownian motion

ABSTRACT

Particle tracking in soft materials allows one to characterise the material's local viscoelastic response, a technique referred to as microrheology (MR). In particular, MR can be especially powerful to ponder the impact of structural ordering on the tracer's transport mechanism and thus disclose intriguing elements that cannot be observed in isotropic fluids. In this work, we perform Dynamic Monte Carlo simulations of isotropic and liquid-crystalline phases of rod-like particles and employ MR to characterise their linear viscoelastic response. By incorporating tracers of different diameters, we can assess the combined effect of size and ordering across the relevant time and length scales of the systems' relaxation. While the dynamics of small tracers is dramatically determined by the background ordering, sufficiently large tracers have a reduced perception of the medium nanostructure and this difference directly influences the observed MR. Our results agree very well with the picture of a microviscosity increasing with the relevant system length scales, but also suggest the crucial relevance of long-ranged order as a key element governing the system's viscoelastic response.

1. Introduction

Soft Matter comprises an especially rich family of physical systems whose structural properties can be altered by weak external stimuli, generally of the magnitude of thermal fluctuations. These systems include polymers, emulsions, gels, and many other soft materials that display an intricate morphology with characteristic length scales ranging from few nanometers to microns. To gain an insight into their mechanical response, a spectrum of direct and indirect techniques has become available [1], including macroscopic rheology and the more recently established microrheology (MR) [2, 3, 4, 5]. Introduced by the seminal works by Mason and Weitz in the 1990s [2, 3], MR allows one to assess the viscoelastic behaviour of a soft material by tracking and analysing the dynamics of guest tracers (or probe particles) dispersed in it. The work by Mason and Weitz triggered further experimental and theoretical research [6, 7, 8, 9] and eventually led to an important extension of the original MR technique, where a tracer is forced to displace upon application of constant, pulsed or oscillating external forces [10, 11, 12, 13]. Such a technique, referred to as active MR, can capture both the linear and nonlinear viscoelastic regimes, including very intriguing phenomena, such as force thinning, where the effective friction coefficient decreases as the magnitude of the applied force increases [14, 15, 16, 17]. By contrast, passive MR, relating the tracer free diffusion to the system's thermal fluctuations, only provides an insight into the linear viscoelastic response.

Recently, we have developed a simulation technique, referred to as Dynamic Monte Carlo (DMC), that can be applied to investigate the dynamics of Brownian systems under the most general conditions [18, 19, 20, 21, 22, 23, 24] and finally extended it to the study of active MR [17]. The DMC method can be employed to investigate the Brownian dynamics (BD) of complex fluids without the constraint of resolving stochastic or deterministic time trajectories as required, respectively, by Brownian dynamics and Molecular Dynamics simulations. Additionally, it allows one to set separate time steps to independently explore short and long time scales, a feature that is especially convenient in the study of dense colloidal suspensions, which generally exhibit a very slow structural relaxation decay. We stress, however, that the current DMC formulation does not explicitly model the solvent, therefore, fluid-mediated hydrodynamic interactions (HI) are disregarded. In this work we apply DMC simulations to investigate the free diffusion of a probe spherical particle immersed in isotropic and liquid-crystalline phases of hard rods. Our specific goal is understanding the effect of the background ordering on the linear viscoelastic response of the system, by explicitly calculating the elastic (G') and viscous (G'') moduli. To this end, we have here investigated colloidal systems comprising anisotropic particles that, at sufficiently large densities, are able to self-assemble into ordered mesophases, such as nematic (N) and smectic (Sm) liquid crystals (LCs). The former display a merely orientational order, whereas the latter are characterised by orientational and positional order. Therefore, such colloidal LCs are especially suitable model systems to gain an insight into the impact of nanostructured ordering on the MR of soft materials. Additionally, we are also interested in clarifying the impact of the tracer size on

*Corresponding author
fabian.garciadaza@manchester.ac.uk (F.A. García Daza); apatti@ugr.es (A. Patti)
ORCID(s): 0000-0002-8473-8349 (F.A. García Daza); 0000-0003-4127-1424 (A.M. Puertas); 0000-0003-2170-0535 (A. Cuetos); 0000-0002-7535-0000 (A. Patti)

the properties of the local structure (microstructure) that is accessible by MR and that is strictly related to the extension of the system's characteristic length scales.

Recently, MR has been employed to ponder the existence of smectic tactoids in N phases of bent-core molecules [25] and shed light on the differences with macroscopic rheology in lamellar, cubic and hexagonal LCs formed in water-monoglyceride mixtures [26]. Nevertheless, these experimental works did not explore how a change in the tracer size could produce different MR responses. In the present work, we show that the local viscoelastic behaviour of a soft material strongly depends on the tracer's perception of the surrounding environment and that this can only be fully understood if one considers the length scales characterising the structural ordering of the host phase in relation to the tracer size. We notice that a theory describing the dependence of the dynamics of a tracer on the relevant length scales of a polymer solution was proposed by Cai et al. [8]. These authors identified three separate regimes that are set on the basis of the ratio between the tracer diameter, d_t, and the characteristic length scales of the polymer matrix, which basically are the distance, ξ, between two chains and the distance, L_e, between their entanglements. The three regimes comprise: *(i)* the motion of small particles ($d_t < \xi$) when unaffected by the surrounding host polymers; *(ii)* the diffusion of intermediate sized particles ($\xi < d_t < L_e$) which is correlated to local polymer motion; and *(iii)* the mobility of larger particles ($d_t > L_e$) being influenced by polymers' entanglements. These length-scales are clearly related to the polymer chain conformations, but ultimately also to the polymer concentration and polymer-solvent interactions. Briefly, upon increasing d_t, the tracer should experience an increasing local viscosity that would eventually saturate to the value of the bulk viscosity when $d_t > L_e$. This theoretical framework would provide information on the fluid local viscosity on the scale of the probe particle and, if this was sufficiently large, also on the fluid bulk viscosity (macroviscosity). Nevertheless, this intriguing scenario does not necessarily reproduce what experiments indicate [27]. Other works have used empirical expressions to fit the experimental data [28, 29], applied to different systems, including polymers [28] and living cells [30]. To the best of our knowledge, none of these expressions incorporate the effect of long-range ordering, which, as we will show here, cannot *a priori* be neglected.

Our paper is organised as follows. In Section 2, we introduce the DMC-based simulation technique for the study of passive MR in a bath of colloidal hard rods. Specific details on DMC have been discussed elsewhere and here we will only remind the key concepts and equations that are functional to the present study. In Section 3, we discuss the effect of tracer size and phase ordering on the viscoelastic behaviour of isotropic (I), nematic (N), and smectic (Sm) colloidal LCs. We report the effective viscosity and the elastic and viscous moduli calculated along the relevant directions of symmetry. Finally, in Section 4, we wrap our conclusions.

2. Model and Simulations

The systems studied in this work consist of a spherical tracer immersed in a host phase comprising rod-like particles. While the bath particles are modelled as hard spherocylinders with length-to-diameter ratio $L^* \equiv L/\sigma = 5$ (see Fig. 1(a)), the tracer is a hard spherical particle with diameter $d_t \geq 0.5\sigma$. In our simulations, the colloidal suspensions comprise $N_r = 1400$ host particles and $N_t = 1$ spherical tracer. We use $k_B T$, σ, and $\tau = \sigma^2/D_0$ as our energy, length and time units, with k_B Boltzmann's constant, T the absolute temperature, $D_0 = k_B T/(\eta_s \sigma)$ and η_s the viscosity coefficient of the solvent. The rod diameter, σ, is maintained constant, while the tracer diameter, d_t, is a simulation parameter that varies between 0.5σ and 8σ. In this work, we are interested in the dynamics of the tracer particle immersed in a bath of rods forming I, N, and Sm phases. It should be pointed out that despite the important role solvent-mediated HI may play on the dynamics of tracer and bath particles, simulating HI within DMC is beyond the scope of this work. Prior to simulate particles dynamics, we first run MC simulations in the canonical ensemble to equilibrate the systems at the volume fractions $\phi = 0.35$, $\phi = 0.45$, and $\phi = 0.51$, corresponding to stable I, N, and Sm phases, respectively [31]. The volume fraction is defined in terms of the volume of a rod, v_r, that of a tracer, v_t, and that of the simulation box, V, and reads $\phi = (N_r v_r + v_t)/V$, where $v_r = \pi\sigma^3/6 + \pi\sigma^2 L/4$, and $v_t = \pi d_t^3/6$. Typical equilibrated snapshots of I, N, and Sm phases of rod-like particles incorporating a spherical tracer of size $d_t = 3\sigma$ are provided in Fig. 1.

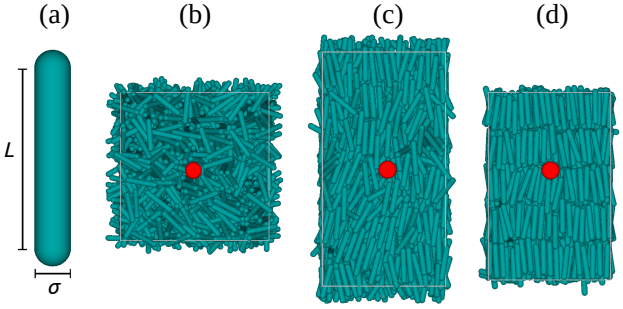

Figure 1: (colour on-line) (a) Example of a typical spherocylinder with length L and diameter σ. Snapshots of a tracer of size $d_t = 3\sigma$ immersed in a colloidal suspension of hard spherocylinders in (a) isotropic ($\phi = 0.35$), (b) nematic ($\phi = 0.45$), and (c) smectic ($\phi = 0.51$) phases.

To monitor the system's long range orientational order, we calculated the nematic and smectic order parameters. The nematic order parameter, S_2, and the nematic director, $\mathbf{n}$, correspond to the largest eigenvalue and its corresponding eigenvector, of the following nematic order parameter tensor

$$Q_{\alpha\beta} = \frac{1}{2N_r} \sum_{j=1}^{N_r} \left(3\hat{\mathbf{u}}_{j\alpha} \cdot \hat{\mathbf{u}}_{j\beta} - \delta_{\alpha\beta}\right), \quad (1)$$

where $\hat{\mathbf{u}}_{j\alpha}$ are unit vectors indicating the orientation of the particle j, $(\alpha, \beta) = \{x, y, z\}$, and $\delta_{\alpha\beta}$ is the Kronecker delta.

High values of the nematic order parameter allow one to distinguish between ordered and disordered phases. Nevertheless, this parameter does not allow a clear distinction to be made between N and Sm phases. To address this, we estimated the smectic order parameter, λ, which reads [32]

$$\lambda = \max_{l} \left\langle \frac{1}{N_r} \left| \sum_{j=1}^{N_r} e^{2\pi i \mathbf{r}_j \cdot \mathbf{n}/l} \right| \right\rangle, \tag{2}$$

where i is the imaginary unit, $\mathbf{r}_j$ the vector position of particle j, and l, the layer spacing, is the value that maximises λ. We have monitored the evolution of nematic and smectic order parameters until a plateau is reached and only fluctuations within a stable window are observed. From equilibrium MC simulations, we observed that $S_2 \approx 0.04$ and $\lambda \approx 0.05$ for the I phase, $S_2 \approx 0.79$ and $\lambda \approx 0.09$ for the N phase, and $S_2 \approx 0.94$ and $\lambda \approx 0.77$ for the Sm phase. The differences between N and Sm phases have been also confirmed by the calculation of several distribution functions. We also notice that no substantial changes in the order parameters were detected at different diameters of the tracer particle.

Equilibrium configurations were then employed to investigate the microrheology of the systems. In particular, the dynamics of the tracer and host particles was assessed by performing DMC simulations in the canonical ensemble and in cuboidal boxes with periodic boundaries. The interested reader is referred to Refs. [18, 19, 20, 22] for specific details on the DMC method. Since our aim is to model realistic time trajectories of the particles, unphysical moves like cluster moves, swaps and jumps are not allowed. A DMC cycle corresponds to $N_p \equiv N_r + N_t$ random attempts to displace and rotate the particles of the system, rotations being only attempted for rods. These movements are accepted or rejected according to the Metropolis algorithm, with probability $\min\left[1, \exp(-\Delta E/k_{\mathrm{B}}T)\right]$, where ΔE is the change in energy resulting from the movement of the particle. Since particle-particle interactions are modelled *via* a hard-core potential, attempted moves are always accepted unless an overlap is detected. In particular, to determine the occurrence of overlaps between rods, we implemented the algorithm proposed by Vega and Lago [33]. The position of the tracer is updated by decoupling its displacement, $\delta\mathbf{r}_t$, into three contributions, where $\delta\mathbf{r}_t = X_x\hat{\mathbf{x}} + X_y\hat{\mathbf{y}} + X_z\hat{\mathbf{z}}$. The magnitude of the attempted displacements is chosen at random with the condition $|X_\alpha| \leq \delta r$, with $\alpha = \{x, y, z\}$. Analogously, the displacement of a rod-like particle reads $\delta\mathbf{r}_r = X_\parallel\hat{\mathbf{u}}_r + X_{\perp,1}\hat{\mathbf{v}}_{r,1} + X_{\perp,2}\hat{\mathbf{v}}_{r,2}$, where $\hat{\mathbf{u}}_r$ represents a unit vector parallel to the main rod axis, whereas $\hat{\mathbf{v}}_{r,m}$, with $m = 1, 2$, are two random unitary vectors perpendicular to $\hat{\mathbf{u}}_r$ and to each other. The magnitude of the rods' displacements along the main particle axes is selected within uniform distributions fulfilling $|X_\parallel| \leq \delta r_\parallel$ and $|X_{\perp,m}| \leq \delta r_\perp$. The maximum displacements, δr, $\delta r_\parallel$ and $\delta r_\perp$, depend on the translational diffusivities of the particles at infinite dilution. For the spherical tracers, this is expressed as:

$$\delta r = \sqrt{2D_t\delta t_{\mathrm{MC},t}} \tag{3}$$

where D_t and $\delta t_{\mathrm{MC},t}$ are, respectively, the diffusion coefficient of the tracer at infinite dilution and its time step in the MC time scale. Similarly, the rods' maximum displacements are given by:

$$\delta r_\parallel = \sqrt{2D_{r,\parallel}\delta t_{\mathrm{MC},r}} \tag{4}$$

$$\delta r_\perp = \sqrt{2D_{r,\perp}\delta t_{\mathrm{MC},r}} \tag{5}$$

where $\delta t_{\mathrm{MC},r}$ is the MC time step for a rod particle, and $D_{r,\parallel}$ and $D_{r,\perp}$ represent its parallel and perpendicular diffusivities at infinite dilution, respectively. In the case of rotations, the orientation vector of the bath particles varies from $\hat{\mathbf{u}}_r$ to $\hat{\mathbf{u}}_r + \delta\hat{\mathbf{u}}_r$, where $\delta\hat{\mathbf{u}}_r = Y_{\varphi,1}\hat{\mathbf{w}}_{r,1} + Y_{\varphi,2}\hat{\mathbf{w}}_{r,2}$, being the vectors $\hat{\mathbf{w}}_{r,m}$ arbitrary chosen in such a way that they are perpendicular to each other and to $\hat{\mathbf{u}}_r$. The maximum rotations must satisfy $|Y_{\varphi,m}| \leq \delta\varphi$, where,

$$\delta\varphi = \sqrt{2D_{r,\varphi}\delta t_{\mathrm{MC},r}} \tag{6}$$

with $D_{r,\varphi}$ is the particle rotational diffusion coefficient at infinite dilution. For both spherical particles and spherocylinders we have disregarded rotations around their axes of angular symmetry. The inclusion of such rotations and their effects on the particles' dynamics are beyond the scope of this study.

The translational diffusion coefficient of the tracer at infinite dilution, D_t, is estimated from the Stokes-Einstein equation. In this work, we have considered tracers of different diameters, $d_t \geq 0.5\sigma$. Therefore, the diffusivity of the tracer is given by:

$$D_t = \frac{D_0}{3\pi}\frac{\sigma}{d_t}. \tag{7}$$

By contrast, the rods' rotational and translational diffusion coefficients at infinite dilution have been estimated by employing the analytical expressions based on the induced-force method for uniaxial particles proposed by Bonet Avalos et al. [34]:

$$\frac{D_{r,\perp}}{D_0} = \frac{\ln(2/\epsilon) - 1/2 - I^{tt}}{2\pi/\epsilon} \tag{8}$$

$$\frac{D_{r,\parallel}}{D_0} = \frac{\ln(2/\epsilon) - 3/2 - I^{tt}}{\pi/\epsilon} \tag{9}$$

$$\frac{D_{r,\varphi}}{D_0} = 3\frac{\ln(2/\epsilon) - 11/6 - I^{rr}}{\pi\sigma^2/(2\epsilon)^3} \tag{10}$$

where $1/\epsilon = 2(L^* + 1)$, $I^{tt} = 0.5\int_{-1}^{1} dx \ln h(x) \simeq -0.0061$ and $I^{rr} = 1.5\int_{-1}^{1} dx x^2 \ln h(x) \simeq -0.017$, with $h(x) = (1 - x^{16})^{1/16}$ a parametric function used to model spherocylinders with symmetry of revolution. The values of the so-calculated translational and rotational diffusion coefficients are reported in Table 1. For a multicomponent system at equilibrium, the Brownian dynamics time can be recovered from the rescaling of the MC time of the individual components as follows [19]

$$\delta t_{\mathrm{BD}} = \frac{\mathcal{A}_t}{3}\delta t_{\mathrm{MC},t} = \frac{\mathcal{A}_r}{3}\delta t_{\mathrm{MC},r} \tag{11}$$

Table 1
Diffusion coefficients at infinite dilution of spherocylinders with aspect ratio $L^* = 5$, calculated from Eqs. 8-10.

$D_{r,\perp}/D_0$	$D_{r,\parallel}/D_0$	$D_{r,\varphi}\sigma^2/D_0$
$3.560 \cdot 10^{-2}$	$4.467 \cdot 10^{-2}$	$6.020 \cdot 10^{-3}$

where $\mathcal{A}_t$ and $\mathcal{A}_r$ are, respectively, the acceptance rates of the tracer and rod-like particles computed at fixed MC time steps $\delta t_{t,\mathrm{MC}}$ and $\delta t_{r,\mathrm{MC}}$. Eq. 11 indicates that, although the two species in the system have different MC timescales, these must re-scale to the same BD timescale. What we practically do is setting the MC time step of the rods and determine the MC time step of the tracer as well as $\mathcal{A}_t$ and $\mathcal{A}_r$ by running short trial-and-error simulations until Eq. 11 converges. By following this preliminary procedure, one ensures that the BD timescale is recovered. Specifically, we have set the DMC time step of the rods to $\delta t_{\mathrm{MC},r} = 10^{-2}\tau$ for all the systems studied and recalculated the time step of the tracer particles as $\delta t_{\mathrm{MC},t} = \delta t_{\mathrm{MC},r}\mathcal{A}_r/\mathcal{A}_t$. Details of the systems studied in this work are shown in Table S1 of the Supplementary Material (SM). This rescaling is of utmost importance to determine the mean-square displacement (MSD) of the tracer particle and hence the viscoelastic response, including elastic and viscous moduli, of the host phase. In particular, the MSD of the tracer is the ensemble average of the particle's displacement from its original position in a given window of time. It is calculated as

$$\langle \Delta r_t^2(t) \rangle = \langle \big(\mathbf{r}_t(t) - \mathbf{r}_t(0)\big)^2 \rangle, \tag{12}$$

where $\mathbf{r}_t$ indicates the position vector of the tracer particle, and the brackets refer to ensemble average over independent trajectories. We have generated 4000 trajectories, each consisting of $6 \cdot 10^5$ MC cycles, to simulate the dynamics of rods and tracer particles in I and N phases. However, it was necessary to run a larger number of cycles ($6 \cdot 10^6$ MC cycles per trajectory) to reach the long-time diffusive regime in Sm phases; in this case, at least 1000 trajectories were used to calculate the ensemble averages.

In passive MR, the tracer's MSD is used to calculate the viscoelastic properties of the system of interest. In particular, the complex shear modulus, $G^*(\omega) = G'(\omega) + iG''(\omega)$, with G' and G'' the elastic and viscous moduli, respectively, in the Fourier domain [6] can be expressed as:

$$G^*(\omega) = \frac{k_\mathrm{B}T}{i\pi\left(d_t/2\right)\omega F\{\langle \Delta r_t^2(t)\rangle\}}, \tag{13}$$

where $\omega = 1/t$ is the time frequency, and $F\{\langle \Delta r_t^2(t)\rangle\}$ is the Fourier transform of the tracer's MSD. In line with the work of Mason [6], the shear modulus can be written as:

$$\left|G^*(\omega)\right| = \frac{k_\mathrm{B}T}{\pi\left(d_t/2\right)\langle \Delta r_t^2(1/\omega)\rangle \Gamma\left[1+\alpha(\omega)\right]}, \tag{14}$$

where $\alpha(\omega) \equiv \left(d\ln\langle \Delta r_t^2(t)\rangle / d\ln(t)\right)|_{t=1/\omega}$ is the local exponent of the MSD, and Γ is the gamma function. Accordingly, elastic and viscous moduli are given, respectively, by:

$$G'(\omega) = \left|G^*(\omega)\right| \cos\left(\frac{\pi\alpha(\omega)}{2}\right), \tag{15}$$

$$G''(\omega) = \left|G^*(\omega)\right| \sin\left(\frac{\pi\alpha(\omega)}{2}\right). \tag{16}$$

In this work, Eqs. 14-16 were employed to assess the viscoelastic behaviour of the host phases from the simulated MSD of the tracer particle. It should be noted that, in addition to the above-mentioned Fourier transform-based method [3, 6], there are other options to infer the viscoelastic response of soft materials from the tracer's MSD, including compliance-based [35, 36] and Laplace transform-based [2] methods. In Fig. S1 of the SM, we show that the viscous and elastic moduli obtained with Eqs. 13-16 and with the compliance-based method proposed by Evans et al. [35] are in excellent agreement.

For a viscous isotropic medium the motion is dominantly diffusive ($\alpha(\omega) \approx 1$) and G'' dominates over G'. By contrast, in an elastic medium the motion is restricted by the local structure of the host phase ($\alpha(\omega) \ll 1$) and G' becomes prominent while G'' vanishes. These tendencies are not only limited to isotropic materials, but are also expected in systems exhibiting orientational or positional order (*e.g.* N and Sm phases). Indeed, in order to have more detailed information on the viscoelastic properties of ordered phases, we have estimated the elastic and viscous moduli in the directions parallel and perpendicular to the nematic director as detailed in the subsequent sections.

3. Results

In this section, we investigate the combined effect of size and structural order on the linear viscoelastic response of soft materials as probed by passive MR. To this end, we have employed colloidal suspensions of rod-like particles, here modelled as hard spherocylinders, which, by forming N and Sm LCs, allow one to ponder the implications of nanostructured ordering and associated symmetry breaking on the MR response. Hard spherocylinders exhibit a very rich phase behaviour [31]; upon increasing the number density of particles, or volume fraction, the system first breaks orientational symmetry and self-assemble into N phases, then positional ordering in one dimension and forms Sm phases, and finally, a crystal phase is found upon further increasing density. Here we explore the rheological behaviour of a system of rod-like particles with passive MR, incorporating spherical tracers of different sizes, as described above. In the isotropic fluid, the effect of the tracer size is studied in more detail, discussing in particular the microviscosity as a function of the tracer size, whereas we focus on the different components of the elastic and viscous moduli in N and Sm LCs.

3.1. Effect of the size of the probe on the viscoelastic behaviour of dense colloidal suspensions

In Fig. 2, we report the elastic and viscous moduli for the isotropic fluid, obtained from the tracer's MSD, with tracer

diameters ranging from 0.5σ to 8σ. The corresponding errors are estimated by G' and G'' assessed from the MSDs of the tracer particles with their associated errors in both limits, $\langle \Delta r_t^2(t)\rangle + \delta\langle \Delta r_t^2(t)\rangle$, and $\langle \Delta r_t^2(t)\rangle - \delta\langle \Delta r_t^2(t)\rangle$ where $\delta\langle \Delta r_t^2(t)\rangle$ indicates the standard error at time t of the averaged MSDs. The top panel shows G' and G'' for the smallest and largest tracer diameter, that is $d_t = 0.5\sigma$ and 8σ. The elastic and viscous moduli resulting from intermediate tracer sizes exhibit a similar behaviour. One can observe an increase of both viscous and elastic response as measured by larger tracers, but the profile of both moduli changes only moderately, keeping the same qualitative behaviour. In particular, for each tracer diameter studied here, G'' is larger than G' across the whole spectrum of time frequencies, revealing the basically viscous response of a fluid-like bath. These tendencies are explored in more detail in the bottom panel of the same figure, where we plot the ratio $\mathcal{R} \equiv G''/G'$, also referred to as loss tangent [37], which reflects the liquid-like ($\mathcal{R} \gg 1$) and solid-like ($\mathcal{R} \ll 1$) nature of the host phase. Although this ratio is larger than one for all cases, as expected, it decreases upon increasing the tracer size, suggesting that the system is indeed fluid-like at small frequency scales ($G'' > 10G'$), but becomes viscoelastic at intermediate scales ($G'' \approx 2G'$ for $\omega/\tau^{-1} \sim 1$), until a more viscous behaviour at larger frequencies is reached again.

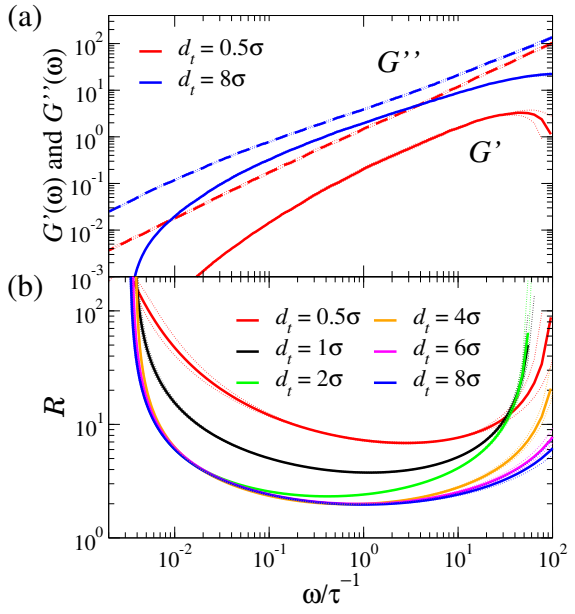

Figure 2: (colour on-line) Top panel: viscous (G'', dashed lines) and elastic (G', solid lines) moduli of a bath of hard spherocylinders in an isotropic phase containing a spherical tracer of diameter 0.5σ (red curves) and 8σ (blue curves). Bottom panel: loss tangent, $\mathcal{R} \equiv G''/G'$, for different diameters of the tracer. Estimated errors are delimited by the dotted lines.

Interestingly enough, while for the smaller tracers there is a marked difference in the loss tangent, for sufficiently large tracers, namely for $d_t \geq 2\sigma$, the loss tangent *vs* frequency profile tends to progressively saturate and to collapse on a single master curve. This tendency denotes the threshold of the tracer size above which the probe starts to notice the bath particles in its immediate vicinity more readily than the (implicit) solvent molecules. For large tracers, this saturation is anticipated at small frequencies, corresponding to long time scales, when tracer motion is distinctly diffusive and the viscous modulus prevails. Both viscous and elastic moduli, however, exhibit a tendency to plateau at intermediate frequencies with the size of the tracer, causing the loss tangent to converge to a single curve. Nevertheless, convergence of $\mathcal{R}$ is not obvious at higher frequencies or, equivalently, shorter timescales, with size effects becoming more and more relevant. Since at short times tracers are still confined within the cage of their nearest neighbours, the contribution of their elastic modulus becomes larger with the tracer size and the loss tangent decreases progressively until merging into a single curve. This overall saturation apparently corresponds to the "bulk" behaviour, as seen by microrheology, which does not necessarily correspond to macroscopic rheology, as we shall see below.

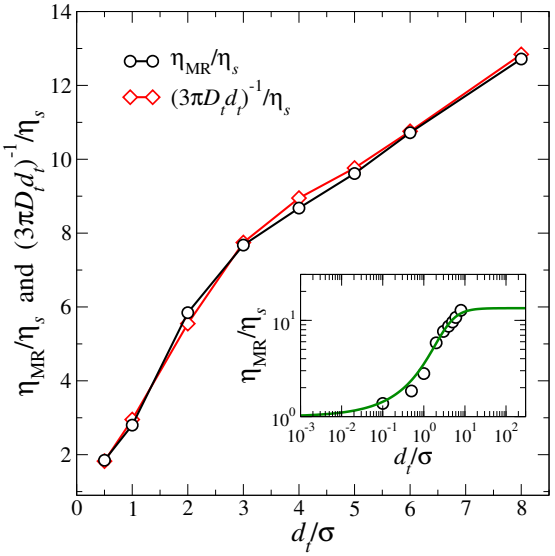

Figure 3: (colour on-line) Effective viscosity *vs* tracer size for systems in the isotropic phase. Microviscosities obtained from the viscous modulus at short frequencies ($\eta_{MR} \sim G''(\omega)/\omega|_{\omega\to 0}$) and the Stokes-Einstein equation at long times are represented by empty circles and diamonds, respectively. The inset compares the microviscosities obtained by our simulations (empty circles) to the model of Kalwarczyk and coworkers [28, 29] (solid line). Absolute errors are smaller than the size of the symbols.

The microviscosity of the bath can be obtained from the small frequency behaviour of the viscous modulus, $G''(\omega \to 0) \sim \eta_{MR}\omega$. The results, as a function of the tracer diameter, are presented in Fig. 3 and compared to the results from the Stokes-Einstein relation using the long-time self-diffusion coefficient obtained from the simulated MSD of the tracer particle, available in Fig. S5 of SM. Please note that as the size of the tracer decreases its interaction with the solvent medium is favoured and η_{MR} approaches η_s. Conversely, large tracers perceive the bath particles more effortlessly and the vis-

cosity they probe increases notably such that $\eta_{\mathrm{MR}}/\eta_s \gg 1$. Nonetheless, both results agree very well on how the tracer size influences microviscosity, which grows steadily with no evidence of saturating to a bulk-like plateau. Similar results have been previously obtained for a bath of colloidal spheres, measured with active MR [38], highlighting that MR should be employed cautiously to estimate the shear viscosity of the bath, at least within this range of tracer sizes. Analogously, the monotonic increase of viscosity with tracer size has been reported in simulations of polymer melts [39] and experiments on dilute suspensions of rod-like *fd*-viruses at specific concentration ranges [40]. The analysis of the results in Figs. 2 and 3 provides further support to MR as a technique on its own to measure the mechanical response of the system to microscopic stresses, but not as a substitute to macroscopic rheology. According to Squires [41], the reason for this difference is that in MR the stress field induced by the moving tracer is not affine, contrary to the case of macroscopic rheology.

Finally, we apply a pseudo-empirical model derived by Kalwarczyk and coworkers for the diffusion of tracers in polymer matrices [28, 29]. This model describes the dependence of microviscosity on the system characteristic lengths as an exponential law of the type $\eta_{\mathrm{MR}} = \eta_s \exp\left[\left(R_{\mathrm{eff}}/\xi\right)^a\right]$, where R_{eff} is the effective radius of the tracer, $\xi = 0.32\sigma$ marks the mean free distance between the host phase elements, and $a = 0.56$ is an exponent of order one. The interested reader is referred to Section S5 of SM for additional details on the calculation of these parameters. The optimal fitting curve is shown in the inset of Fig. 3 (continuous green line). The model describes correctly the microviscosity measured in the simulations (empty circles), and predicts a saturation outside the range of tracer sizes studied here. A similar saturation has also been observed in experiments of polystyrene nanoparticles within polymeric matrices of partially hydrolyzed polyacrylamide [42], and in dilute suspensions of rod-like viruses with $L^* \equiv L/\sigma = 133$ in the presence of spherical tracers of size comparable to the characteristic lengths of the host particles ($64 \leq d_t/\sigma \leq 152$) [40].

3.2. Effect of orientational order on the viscoelastic properties of dense colloidal suspensions

Liquid-crystalline phases exhibit long range orientational order, which is characterised by the nematic director. Ordering affects the overall mechanical properties, but most prominently breaks the bath isotropy. To gain an insight into the effect of the order on the mechanical properties of the N and Sm phases, we have calculated their elastic and viscous moduli at tracer diameters between $d_t = 1\sigma$ and 3σ. Similarly to the tendencies observed in the I phase, both G' and G'' increase with the tracer size (Figs. S3 and S4 of SM). Indeed, G'' is larger than G' despite the fact that N and Sm LCs are denser than the I phase discussed previously. Nevertheless, their loss tangent, $\mathcal{R} \equiv G''/G'$, shown in Fig. S7 of SM, exhibits a decrease upon increasing tracer size, with the profiles tending to collapse on a single curve at intermediate frequencies. Although all loss tangents confirm the dominant viscous nature of nematics and smectics, it is clear that N and Sm LCs are perceived more and more solid-like by larger tracers.

In passive MR, the anisotropic diffusion of the tracer can be translated to different behaviours of the moduli in the parallel and perpendicular directions to the nematic director. This opens up even more the possibility of assessing the effect of positional and orientational order on the viscoelastic properties of the N and Sm LCs which is certainly intriguing and will be tackled below. Following the work by Hasnain and Donald [43], the tracer's MSD parallel, $\Delta r^2_{t,\parallel}$, and perpendicular, $\Delta r^2_{t,\perp}$, to the nematic director may be used to estimate the parallel ($G'_\parallel$, $G''_\parallel$) and perpendicular ($G'_\perp$, $G''_\perp$) components of the elastic and viscous moduli. In the N phase, regardless the tracer size, the perpendicular component of both elastic and viscous moduli is larger than the component along the nematic director (Fig. S8 of SM). Similar observations were reported by Habibi et al. [44] in experiments of disodium chromoglycate solutions displaying N phases. In our case, this difference is caused by the tracer's anisotropic diffusion, being more hindered in the perpendicular direction due to the barrier imposed by the oriented rods. Thereby, the system exhibits a more solid-like in the perpendicular direction, with $G'_\perp > G'_\parallel$. Nonetheless, we notice that for sufficiently large tracers, the difference between both moduli becomes more and more subtle, indicating that the system is more isotropic as seen by larger tracers. This is a consequence of the space perturbation caused by the tracer, breaking the nematic order on its surroundings and "probing" a locally isotropic system.

An equivalently comprehensive analysis can be inferred from the parallel ($\mathcal{R}_\parallel \equiv G''_\parallel/G'_\parallel$) and perpendicular ($\mathcal{R}_\perp \equiv G''_\perp/G'_\perp$) components of the loss tangent for the N phase which are depicted in the top panel of Fig. 4. Interestingly, the loss tangents tend to acquire a very similar qualitative and quantitative profile upon increasing tracer size. As such, it is not the individual values of directional G' and G'' that saturate to a plateau, but rather their ratio, which can be considered as an indicator of the occurrence of a local bulk-like behaviour being perceived by the probe particle. Furthermore, Fig. 4(a) highlights an interesting crossover between parallel and perpendicular loss tangents at low frequencies as the tracer diameter increases from 1σ to 2σ. More specifically, $\mathcal{R}_\perp > \mathcal{R}_\parallel$ at $d_t = 1\sigma$, while $\mathcal{R}_\perp < \mathcal{R}_\parallel$ at $d_t \geq 2\sigma$. The low-frequency domain corresponds to the long-time diffusive regime, which dramatically depends on system packing and ordering as well as on tracer size. Although both packing and ordering are the same, tracers of different size perceive the presence of surrounding rods differently and their dynamics adapt to the same environment accordingly. Consequently, while small tracers experience a dominant viscous-like character of nematics in the perpendicular direction, larger tracers see this prevailing viscosity along the nematic director.

Contrary to the nematic case, the parallel components of G' and G'' in smectics (Fig. S9 in SM) are larger than their perpendicular components, most likely due to a less

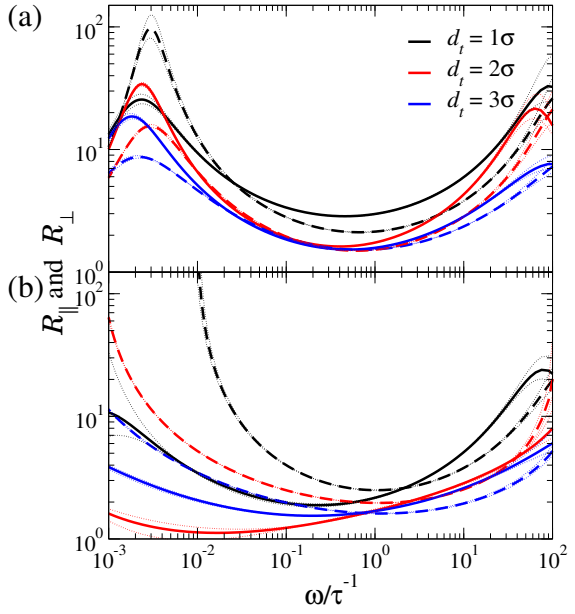

Figure 4: (colour on-line) Loss tangent in the directions parallel ($\mathcal{R}_\parallel = G''_\parallel/G'_\parallel$, solid lines) and perpendicular ($\mathcal{R}_\perp = G''_\perp/G'_\perp$, dashed lines) to the nematic director of a bath of hard spherocylinders in the N (top panel) and Sm (bottom panel) phases with tracer particle diameters 1σ, 2σ, and 3σ represented by black, red, and blue curves, respectively. Estimated errors are delimited by the dotted lines.

hindered diffusion in the perpendicular direction to the nematic director. This somewhat counter-intuitive result is due to the trajectories that tracers preferentially explore while diffusing through Sm LCs. In particular, small tracers spend a significant amount of time in the quasi-2D spacing between contiguous layers, jumping from an inter-layer region to another when random density fluctuations occur, as also already established in the past [45]. By contrast, larger tracers ($d_t = 3\sigma$) experience a smoother diffusion, where abrupt jumps are rarely observed, and perceive the surrounding media, whose global ordering and packing are unchanged, as more homogeneous than it actually is. In other words, the layered arrangement of the Sm phase has moderate impact on the dynamics of the tracer, which breaks the ordering and ends up perceiving a different effective viscoelasticity.

To facilitate interpretation, Fig. 4(b) depicts the loss tangent of the individual moduli components in Sm phase. Noticeably, at low frequencies, $\mathcal{R} \simeq 1$ for $d_t = 2\sigma$ in the parallel direction as shown by the solid red line. This component exhibits a non-monotonic behaviour as a function of the tracer size, whereas it decreases continuously in the perpendicular direction. Also different from the nematic case in Fig. 4(a), the curves do not collapse for large tracers, and the mechanical properties of the system, as probed by the tracer, continue evolving for larger tracers. We believe that the non-monotonic behaviour of the parallel component can also be due to the change in the tracer's dynamics with its size. As a result, diffusion into the layer is most hindered for $d_t = 2\sigma$, causing the smallest G''/G' ratio observed in Fig. 4(b). In any case, it should be noted that the typical indications of viscoelastic behaviour, namely, a plateau in G' and a minimum in G'', are not observed even for the case of $d_t = 2\sigma$ in the parallel component. As a matter of fact, the tracer's MSD does not exhibit the typical intermediate plateau that would prove a localisation length (Fig. S10 in SM).

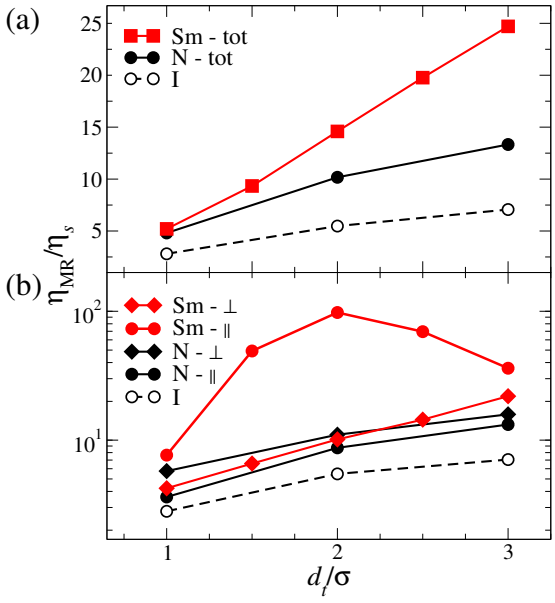

Figure 5: (colour on-line) Microviscosities of a bath of hard spherocylinders in the I (empty symbols), N (black symbols), and Sm (red symbols) phases for different sizes of the tracer particle. Top panel: microviscosity calculated in the three spatial coordinates. Bottom panel: microviscosity in the parallel (∥, solid circles) and perpendicular (⊥, solid diamonds) directions to the nematic vector. Absolute errors are smaller than the size of the symbols.

Finally, the microviscosity obtained from the low-frequency trend of G'' is shown in Fig. 5 for the three phases studied in the 3D case (top panel) as well as the parallel and perpendicular components to the nematic director in the liquid-crystalline phases (bottom panel). According to Fig. 5(a), the isotropic microviscosity is significantly larger in denser states, and grows monotonically with the tracer size but without reaching a plateau. More captivating is the behaviour of the longitudinal and transverse components of microviscosity depicted in Fig. 5(b). In the N phase the perpendicular component exceeds its parallel counterpart and both grow monotonically with the size of the tracer. This is consistent with what has been reported in experiments of spherical probe particles diffusing in nematic suspensions of prolate micelles [46] and *fd*-viruses [47]. Interestingly, the spacing between the parallel and perpendicular microviscosity decreases with increasing the diameter of the probe particle similar to that previously observed in experiments [46]. By contrast, in the Sm phase the perpendicular component is surpassed by the parallel one, which in turn displays a non-monotonic dependence on tracer size. Small tracers do feel the surrounding ordering and naturally accommodate in the region delimited by adjacent smectic layers. Accordingly,

the residence time in the inter-layer region is much longer for tracers with $d_t = 2\sigma$ (Fig. S11 of SM), which results in a lower mobility along the nematic director and explains the non-progressive increase of the microviscosity in this direction. Furthermore, the preference of these tracer particles to remain in the interstitial spaces between the smectic layers favours their mobility across the quasi-2D region between neighbouring layers, leading to a perpendicular microviscosity that is smaller than that detected in N phases, despite the Sm phase being significantly denser.

It is therefore evident that the interplay between the long-range order of the host phase and the relative size of the tracer to the bath particles has a major role to play in predicting the viscoelastic properties of structured fluids. To the best of our knowledge, this has only been discussed in the literature by a limited number of works, particularly from the point of view of MR and numerical simulations [48, 49, 50]. Certainly, empirical scaling laws that neglect long-range ordering might not be able to accurately predict the effective viscosity of tracers diffusing in nanostructured fluids. Our results may have relevant implications in the study of the shear of liquid-crystalline phases or the transport of beads or impurities in nanostructured materials.

4. Conclusions

Microrheology (MR) makes use of tracer particles to provoke local deformations in the host fluid and hence measure its viscoelastic properties on the tracer's characteristic length scales [7, 51]. It is therefore different from macroscopic rheology which probes the material's response over much larger length scales. MR has been successfully applied to the study of colloids [5, 17, 52], polymers [53], gels [54, 55] and biological matter [40, 56]. However, much less attention has been devoted to the implications on MR measurements of the nanostructured ordering and associated symmetry breaking that some of the above-mentioned systems might exhibit. LCs of colloidal particles are excellent model systems to ponder the effect of orientational and positional ordering on the viscoelastic response along the relevant directions.

We notice that former experiments applied MR to molecular and lyotropic LCs to study, respectively, the formation of smectic domains in nematics of bent-core molecules [25] and how viscoelasticity probed by MR compares to that probed by macroscopic rheology [26]. However, these experiments employed single-sized probes, neglecting how smaller or larger tracers could perceive the order of the surrounding nanostructured fluid, adapt their dynamics and eventually produce distinct MR responses. The hypothesis that triggered the present work was that only by scaling the characteristic lengths of the host phase to the tracer size would it be possible to have a full insight into the linear viscoelastic response of a nanostructured fluid as probed by passive MR.

To test this hypothesis, we have performed DMC simulations of isotropic and liquid-crystalline phases of colloidal hard rods. Our goal was assessing the combined effect of phase ordering and tracer size on the system response across the relevant time scales of its structural relaxation. The key lesson that can be learnt is that structure, dynamics and MR are intimately correlated and, only if gauged with each other, can pave the path to a comprehensive understanding of the viscoelastic behaviour of complex fluids. The striking evidence of this apparently obvious conclusion is given by the analysis of the microviscosity in the Sm phase. Its non-monotonic dependence on the tracer size along the phase director suggests that the effect of phase ordering should not be neglected and that empirical scaling laws, merely based on geometrical considerations, might not be especially accurate when assessing MR in nanostructured fluids [28, 29, 30]. The impact of long-ranged order is also fully appreciated when calculating the microviscosity experienced by the probe particle at low frequencies, that is when $\eta_{\mathrm{MR}} \sim G''(\omega \to 0)/\omega$. More specifically, perpendicularly to the phase director, the microviscosity of relatively small tracers ($d_t \leq 2\sigma$) in the N phase was found to be larger than that in the Sm phase. This was ascribed to the typical arrangement of positionally-ordered LCs, which constrains the tracer to the low-density, quasi-2D region between adjacent smectic layers, thus favouring its diffusion as compared to that observed in merely orientationally-ordered phases. Larger tracers, which can no longer fit in the inter-layer spacing of smectics, end up perceiving a microviscosity that eventually becomes larger than that in the N phase. On the other hand, the microviscosity along the Sm phase director displays an unexpected non-monotonic behaviour. From our analysis, compared to $d_t = 1\sigma$ and 3σ size tracers, the long residence time of tracers with $d_t = 2\sigma$ in the interstitial regions between the layers, substantially diminishes their capability to diffuse through the inter-layers, causing a sharp increase in microviscosity when d_t passes from 2σ to 3σ. It thus results evident that geometrical elements (*e.g.* tracer and system characteristic lengths), while indeed relevant to gain a solid view on the system viscoelastic response, should be assessed within a more inclusive scenario, where long-ranged structural ordering and its implications on tracer mobility play fundamental roles.

The analysis of the loss tangent, $\mathcal{R} \equiv G''(\omega)/G'(\omega)$, indicates that isotropic and liquid-crystalline phases are essentially viscous at small frequencies, but then exhibit a gradually increasing elastic response and mature into viscoelastic at larger frequencies. This tendency results to be dramatically determined by the tracer size in isotropic phases, where from $\mathcal{R} \approx 10$ at $\omega\tau = 1$ it decreases to $\mathcal{R} \approx 2$ upon increasing the tracer diameter from $d_t = 0.5\sigma$ to 8σ. Equally interesting is observing that the loss tangent tends to a plateau for sufficiently large tracers ($d_t \geq 2\sigma$), indicating that a "bulk" behaviour can be eventually achieved within the limits imposed by microrheology, which do not necessarily overlap with those of macroscopic rheology. Similar qualitative and quantitative trends are also found in N and Sm LCs, suggesting that larger and larger tracers have an increasingly reduced perception of the nanostructure of the surrounding medium. In other words, sufficiently large probe particles see the bath as a continuous fluid whose nanostructure is not relevant. This explains why the microviscosity in the Sm phase decreases abruptly when d_t increases from 2σ to 3σ. As a

confirmation of the strong link existing between structure, dynamics and MR, these considerations are consistent with the change in the tracer dynamics that one observes in Sm phases along the director. The rattling-and-jumping dynamics at $d_t = 1\sigma$, with the probe sporadically hopping from one inter-layer region to another, transforms into a merely rattling dynamics at $d_t = 3\sigma$, with the probe effectively missing the presence of a layered structure.

Finally, we would like to stress that DMC simulations neglect the fluid-mediated hydrodynamic interactions between tracer and bath particles, which might have a non-negligible impact on diffusive properties and consequently on MR [40]. While this impact is expected to be especially relevant if tracers were much smaller than the mesh size of the network of rods [40, 57], which is not the case explored here, we are currently working on a new version of the DMC technique that will incorporate HI effects and eventually provide an additional degree of precision to the measurements reported here. A step in this direction would imply to treat HI within the induced force method [34, 58], which estimates the effect on the mobility of each particle due to the presence of its surrounding neighbours. Each particle's mobility matrix is related to integrals of the Oseen tensor over particle surfaces, which can be evaluated numerically. The main advantage of this methodology is that the mobility matrices can be obtained unequivocally for spherical particles as well as for particles with axial symmetry such as spherocylinders.

Acknowledgements

F.A.G.D., A.M.P and A.P. acknowledge the International Exchanges Grant IES\R1\191066, awarded by The Royal Society. F.A.G.D. and A.P. also acknowledge the Leverhulme Trust Research Project Grant RPG-2018-415, and the assistance given by Research IT and the use of the Computational Shared Facility at The University of Manchester. A.M.P. was also funded by the Spanish Ministerio de Ciencia, Innovación y Universidades under project PGC2018-101555-B-I00 and UAL/CECEU/FEDER through project UAL18-FQM-B038-A. A.C was funded by Consejería de Transformación Económica, Industria, Conocimiento y Universidades de la Junta de Andalucía/FEDER through project P20-00816

References

[1] R. G. Larson, The Structure and Rheology of Complex Fluids, Oxford University Press, USA, 1999.

[2] T. G. Mason, D. A. Weitz, Optical measurements of frequency-dependent linear viscoelastic moduli of complex fluids, Phys. Rev. Lett. 74 (1995) 1250–1253.

[3] T. G. Mason, K. Ganesan, J. H. van Zanten, D. Wirtz, S. C. Kuo, Particle tracking microrheology of complex fluids, Phys. Rev. Lett. 79 (1997) 3282–3285.

[4] P. Cicuta, A. M. Donald, Microrheology: a review of the method and applications, Soft Matter 3 (2007) 1449–1455.

[5] A. M. Puertas, T. Voigtmann, Microrheology of colloidal systems, J. Phys.: Condens. Matter 26 (2014) 243101.

[6] T. G. Mason, Estimating the viscoelastic moduli of complex fluids using the generalized stokes–einstein equation, Rheol. Acta 39 (2000) 371–378.

[7] T. M. Squires, T. G. Mason, Fluid mechanics of microrheology, Annu. Rev. Fluid Mech. 42 (2010) 413–438.

[8] L.-H. Cai, S. Panyukov, M. Rubinstein, Mobility of nonsticky nanoparticles in polymer liquids, Macromolecules 44 (2011) 7853–7863.

[9] M. Karim, T. Indei, J. D. Schieber, R. Khare, Determination of linear viscoelastic properties of an entangled polymer melt by probe rheology simulations, Phys. Rev. E 93 (2016) 012501.

[10] A. Khair, J. Brady, Single particle motion in colloidal dispersions: A simple model for active and nonlinear microrheology, J. Fluid Mech. 557 (2006) 73–117.

[11] R. R. Brau, J. M. Ferrer, H. Lee, C. E. Castro, B. K. Tam, P. B. Tarsa, P. Matsudaira, M. C. Boyce, R. D. Kamm, M. J. Lang, Passive and active microrheology with optical tweezers, J. Opt. A: Pure Appl. Opt. 9 (2007) S103–S112.

[12] M. Gnann, I. Gazuz, A. Puertas, M. Fuchs, T. Voigtmann, Schematic models for active nonlinear microrheology, Soft Matter 7 (2011) 1390–1396.

[13] A. Kuhnhold, W. Paul, Active one-particle microrheology of an unentangled polymer melt studied by molecular dynamics simulation, Phys. Rev. E 91 (2015) 042601.

[14] T. M. Squires, J. F. Brady, A simple paradigm for active and nonlinear microrheology, Phys. Fluids 17 (2005) 073101.

[15] I. C. Carpen, J. F. Brady, Microrheology of colloidal dispersions by brownian dynamics simulations, J. Rheol. 49 (2005) 1483–1502.

[16] I. Gazuz, A. M. Puertas, T. Voigtmann, M. Fuchs, Active and nonlinear microrheology in dense colloidal suspensions, Phys. Rev. Lett. 102 (2009) 248302.

[17] F. A. García Daza, A. M. Puertas, A. Cuetos, A. Patti, Microrheology of colloidal suspensions via dynamic monte carlo simulations, J. Colloid Interface Sci. 605 (2022) 182–192.

[18] A. Patti, A. Cuetos, Brownian dynamics and dynamic monte carlo simulations of isotropic and liquid crystal phases of anisotropic colloidal particles: A comparative study, Phys. Rev. E 86 (2012) 011403.

[19] A. Cuetos, A. Patti, Equivalence of brownian dynamics and dynamic monte carlo simulations in multicomponent colloidal suspensions, Phys. Rev. E 92 (2015) 022302.

[20] D. Corbett, A. Cuetos, M. Dennison, A. Patti, Dynamic monte carlo algorithm for out-of-equilibrium processes in colloidal dispersions, Phys. Chem. Chem. Phys. 20 (2018) 15118–15127.

[21] M. Chiappini, A. Patti, M. Dijkstra, Helicoidal dynamics of biaxial curved rods in twist-bend nematic phases unveiled by unsupervised machine learning techniques, Phys. Rev. E 102 (2020).

[22] F. A. García Daza, A. Cuetos, A. Patti, Dynamic monte carlo simulations of inhomogeneous colloidal suspensions, Phys. Rev. E 102 (2020) 013302.

[23] A. Patti, A. Cuetos, Dynamics of colloidal cubes and cuboids in cylindrical nanopores, Physics of Fluids 33 (2021) 097103.

[24] L. Tonti, F. A. García Daza, A. Patti, Diffusion of globular macromolecules in liquid crystals of colloidal cuboids, J. Mol. Liq. 338 (2021) 116640.

[25] S. Paladugu, S. Kaur, G. Mohiuddin, R. Pujala, S. Pal, S. Dhara, Microrheology to probe smectic clusters in bent-core nematic liquid crystals, Soft Matter 16 (2020) 7556–7561.

[26] M. M. Alam, R. Mezzenga, Particle tracking microrheology of lyotropic liquid crystals, Langmuir 27 (2011) 6171–6178. PMID: 21510686.

[27] D. Langevin, F. Rondelez, Sedimentation of large colloidal particles through semidilute polymer solutions, Polymer 19 (1978) 875–882.

[28] T. Kalwarczyk, N. Ziębacz, A. Bielejewska, E. Zaboklicka, K. Koynov, J. Szymański, A. Wilk, A. Patkowski, J. Gapiński, H.-J. Butt, R. Hołyst, Comparative analysis of viscosity of complex liquids and cytoplasm of mammalian cells at the nanoscale, Nano Lett. 11 (2011) 2157–2163.

[29] T. Kalwarczyk, K. Sozanski, A. Ochab-Marcinek, J. Szymański, M. Tabaka, S. Hou, R. Hołyst, Motion of nanoprobes in complex liquids within the framework of the length-scale dependent viscosity model, Adv. Colloid Interface Sci. 223 (2015) 55–63.

[30] G. Bubak, K. Kwapiszewska, T. Kalwarczyk, K. Bielec, T. Andryszewski, M. Iwan, S. Bubak, R. Hołyst, Quantifying

nanoscale viscosity and structures of living cells nucleus from mobility measurements, J. Phys. Chem. Lett. 12 (2021) 294–301.
[31] P. Bolhuis, D. Frenkel, Tracing the phase boundaries of hard spherocylinders, J. Chem. Phys. 106 (1997) 666–687.
[32] M. Cifelli, G. Cinacchi, L. De Gaetani, Smectic order parameters from diffusion data, The Journal of Chemical Physics 125 (2006) 164912.
[33] C. Vega, S. Lago, A fast algorithm to evaluate the shortest distance between rods, Comput. Chem. 18 (1994) 55 – 59.
[34] J. Bonet Avalos, J. Rubí, D. Bedeaux, G. van der Zwan, Friction coefficients of axisymmetric particles in suspension, Phys. A 211 (1994) 193 – 217.
[35] R. M. L. Evans, M. Tassieri, D. Auhl, T. A. Waigh, Direct conversion of rheological compliance measurements into storage and loss moduli, Phys. Rev. E 80 (2009) 012501.
[36] K. Nishi, M. L. Kilfoil, C. F. Schmidt, F. C. MacKintosh, A symmetrical method to obtain shear moduli from microrheology, Soft Matter 14 (2018) 3716–3723.
[37] E. Furst, T. Squires, Microrheology, Oxford University Press, 2018. doi:10.1093/oso/9780199655205.001.0001.
[38] F. Orts, G. Ortega, E. M. Garzón, M. Fuchs, A. M. Puertas, Dynamics and friction of a large colloidal particle in a bath of hard spheres: Langevin dynamics simulations and hydrodynamic description, Phys. Rev. E 101 (2020) 052607.
[39] A. Kuhnhold, W. Paul, Passive one-particle microrheology of an unentangled polymer melt studied by molecular dynamics simulation, Phys. Rev. E 90 (2014) 022602.
[40] K. Kang, J. Gapinski, M. P. Lettinga, J. Buitenhuis, G. Meier, M. Ratajczyk, J. K. G. Dhont, A. Patkowski, Diffusion of spheres in crowded suspensions of rods, J. Chem. Phys. 122 (2005) 044905.
[41] T. M. Squires, Nonlinear microrheology: Bulk stresses versus direct interactions, Langmuir 24 (2008) 1147–1159.
[42] R. Poling-Skutvik, R. Krishnamoorti, J. C. Conrad, Size-dependent dynamics of nanoparticles in unentangled polyelectrolyte solutions, ACS Macro Lett. 4 (2015) 1169–1173.
[43] I. A. Hasnain, A. M. Donald, Microrheological characterization of anisotropic materials, Phys. Rev. E 73 (2006) 031901.
[44] A. Habibi, C. Blanc, N. Mbarek, T. Soltani, Passive and active microrheology of a lyotropic chromonic nematic liquid crystal disodium cromoglycate, J. Mol. Liq. 288 (2019).
[45] M. Piedrahita, A. Cuetos, B. Martínez-Haya, Transport of spherical colloids in layered phases of binary mixtures with rod-like particles, Soft Matter 11 (2015) 3432–3440.
[46] F. Mondiot, J.-C. Loudet, O. Mondain-Monval, P. Snabre, A. Vilquin, A. Würger, Stokes-einstein diffusion of colloids in nematics, Phys. Rev. E 86 (2012) 010401.
[47] K. Kang, A. Wilk, J. Buitenhuis, A. Patkowski, J. K. G. Dhont, Diffusion of spheres in isotropic and nematic suspensions of rods, J. Chem. Phys. 124 (2006) 044907.
[48] A. K. Tucker, R. Hernandez, Diffusion of a spherical probe through static nematogens: Effect of increasing geometric anisotropy and long-range structure, J. Phys. Chem. B 116 (2012) 1328–1334.
[49] M. Gómez-González, J. C. del Álamo, Two-point particle tracking microrheology of nematic complex fluids, Soft Matter 12 (2016) 5758–5779.
[50] A. Córdoba, T. Stieger, M. G. Mazza, M. Schoen, J. J. de Pablo, Anisotropy and probe-medium interactions in the microrheology of nematic fluids, J. Rheol. 60 (2016) 75–95.
[51] V. Breedveld, D. J. Pine, Microrheology as a tool for high-throughput screening, Journal of Materials Science 38 (2003) 4461–4470.
[52] P. Malgaretti, A. M. Puertas, I. Pagonabarraga, Active microrheology in corrugated channels: Comparison of thermal and colloidal baths, Journal of Colloid and Interface Science 608 (2022) 2694–2702.
[53] T. Gisler, D. A. Weitz, Scaling of the microrheology of semidilute f-actin solutions, Phys. Rev. Lett. 82 (1999) 1606–1609.
[54] B. A. Krajina, C. Tropini, A. Zhu, P. DiGiacomo, J. L. Sonnenburg, S. C. Heilshorn, A. J. Spakowitz, Dynamic light scattering microrheology reveals multiscale viscoelasticity of polymer gels and precious biological materials, ACS Central Science 3 (2017) 1294–1303.
[55] M. E. Szakasits, K. T. Saud, X. Mao, M. J. Solomon, Rheological implications of embedded active matter in colloidal gels, Soft Matter 15 (2019) 8012–8021.
[56] P. C. Cai, B. A. Krajina, M. J. Kratochvil, L. Zou, A. Zhu, E. B. Burgener, P. L. Bollyky, C. E. Milla, M. J. Webber, A. J. Spakowitz, S. C. Heilshorn, Dynamic light scattering microrheology for soft and living materials, Soft Matter 17 (2021) 1929–1939.
[57] K. Kang, A. Wilk, A. Patkowski, J. K. G. Dhont, Diffusion of spheres in isotropic and nematic networks of rods: Electrostatic interactions and hydrodynamic screening, The Journal of Chemical Physics 126 (2007) 214501.
[58] J. Bonet Avalos, J. M. Rubi, D. Bedeaux, Dynamics of rodlike polymers in dilute solution, Macromolecules 26 (1993) 2550–2561.